PCCP

Light-enhanced Oxygen Degradation of $MAPbBr_3$ Single Crystal

Journal:	*Physical Chemistry Chemical Physics*
Manuscript ID	CP-ART-07-2023-003493.R2
Article Type:	Paper
Date Submitted by the Author:	22-Dec-2023
Complete List of Authors:	Wang, Ke; University of Rochester, Ecker, Benjamin; University of Rochester, Physics and Astronomy Ghosh, Maitrayee; University of Rochester Li, Mingze; UNC-Chapel Hill Karasiev, Valentin V.; University of Rochester Laboratory for Laser Energetics Hu, S. X.; University of Rochester Laboratory for Laser Energetics Huang, Jinsong; University of North Carolina at Chapel Hill, Applied Physical Science; University of Nebraska-Lincoln Department of Mechanical Engineering, Gao, Yongli; University of Rochester

ARTICLE

Light-enhanced Oxygen Degradation of $MAPbBr_3$ Single Crystal

Ke Wang[a], Benjamin Ecker[a], Maitrayee Ghosh[b], Mingze Li[c], Valentin V. Karasiev[b], S. X. Hu[b], Jinsong Huang[c], and Yongli Gao[a*]

Received 00th January 20xx,
Accepted 00th January 20xx

DOI: 10.1039/x0xx00000x

Organometal halide perovskites are promising materials for optoelectronic applications, whose commercial realization depends critically on the stability under multiple environmental factors. In this study, methylammonium lead bromide ($MAPbBr_3$) single crystal was cleaved and exposed to simultaneous oxygen and light illumination in ultrahigh vacuum (UHV). The exposure process was monitored using X-ray photoelectron spectroscopy (XPS) with precise control of the exposure time and oxygen pressure. It was found that the combination of oxygen and light accelerated the degradation of $MAPbBr_3$, which could not be viewed as a simple addition of that by oxygen-only and light-only exposures. The XPS spectra showed significant loss of carbon, bromine, and nitrogen at oxygen exposure of 10^{10} Langmuir with light illumination, approximately 17 times of the additive effects of oxygen-only and light-only exposure. It was also found that the photoluminescence (PL) emission was much weakened by oxygen and light co-exposure, while previous reports had shown that PL was substantially enhanced by oxygen-only exposure. Measurements by scanning electron microscope (SEM) and focused ion beam (FIB) demonstrated that the crystal surface was much roughened by the co-exposure. Density functional theory (DFT) calculations revealed formation of superoxide and oxygen induced gap state, suggesting creation of oxygen radicals by light illumination as a possible microscopic driving force for the enhanced degradation.

Introduction

Since its first use as a light-absorbing material in a solar cell, organometal halide perovskites have been attracting a lot of attentions in recent years, with the power conversion efficiency (PCE) rising from 3.3% to 26.1% in 2023.[1-3] Among all perovskites, methylammonium lead halide ($MAPbX_3$) has outstanding optoelectronic properties, including long diffusion length, long carrier lifetime, tunable bandgap, and high absorption coefficient.[4-10] These characteristics not only contribute to its remarkable PCE but also expand its applications to light-emitting diodes, gas detectors, charged particle detectors and photodetectors.[11-17] In particular, $MAPbBr_3$ is considered superior to $MAPbI_3$ in some aspects, as it has higher hole mobility and is more stable than $MAPbI_3$ in air.[18-21] It has also been widely used in the fields of optoelectronics and photovoltaics.[22-25] Especially, its application in X-ray detectors has been reported having an extremely low surface recombination rate and longer diffusion length.[13] However, the perovskites still face some challenges before large-scale commercial use, and the stability of the perovskites is the most critical one. A lot of environmental factors were studied to exam their effects on perovskite stability, such as moisture, heat, gases, and light illumination.[26-36] Substantial amounts of work have been carried out at the device level, which are usually focused on the parameters such as open-circuit voltage (Voc), short-circuit current density (Jsc), fill factor (FF), and PCE.[37-41] Therefore, the mechanisms behind the degradation process still need to be discovered by studying the electronic and chemical properties of the perovskites.

To investigate the stability of $MAPbBr_3$ single crystal at the atomic level, we have performed a series of experiments under different environmental conditions, such as moisture exposure, light exposure, and different gases exposures. It is found that $MAPbBr_3$ single crystal is sensitive to moisture and is initially n-doped by water, then starts to degrade after water exposure reaches a certain threshold. Both nitrogen and oxygen were able to p-dope the crystal. Nitrogen was physisorbed and slowly left the crystal surface afterward, while oxygen could bond with C to form C–O. X-ray-induced degradation was inevitable as the crystal was measured with XPS, which could cause about 10% of perovskite Pb to convert to metallic Pb. Light illumination on the crystal was observed to substantially deteriorate the chemical composition of the crystal and covert about 70% of perovskite Pb to metallic Pb. It even generated voids 1-3 μm below the crystal surface.[30, 32] In addition, Murali *et al.* found that water can form a hydrated layer on $MAPbBr_3$ single crystal surface while the bulk part remained intact.[42] Galisteo-López *et al.* showed that ion migration induced by the light illumination caused structural changes in the crystal lattice.[43] Ouyang *et al.*

[a] *Department of Physics and Astronomy, University of Rochester, Rochester, NY 14627.*
[b] *Laboratory for Laser Energetics (LLE), University of Rochester, Rochester, NY 14623.*
[c] *Department of Applied Physical Sciences, University of North Carolina at Chapel Hill, Chapel Hill, NC, 27599*
† Footnotes relating to the title and/or authors should appear here.
Electronic Supplementary Information (ESI) available: [details of any supplementary information available should be included here]. See DOI: 10.1039/x0xx00000x

revealed photo-oxidative degradation mechanism of $MAPbI_3$ with DFT calculations.[44] However, these degradations were mostly investigated with only one environmental factor except some investigations on spin-coated $MAPbI_3$ thin films.[44-46] The biggest difference between light and oxygen exposure is that the $MAPbBr_3$ single crystal was barely degraded in the oxygen-only exposure, while it was significantly decomposed in the light-only exposure.[30, 32] However, in real applications, multiple environmental factors can act simultaneously and it is critical to investigate and understand whether a simultaneous exposure to multiple factors merely results in a simple addition of the individual exposures or invokes more profound changes and reactions.

Herein, we present our experimental and theoretical investigation on the stability of *in-situ* cleaved $MAPbBr_3$ single crystal under light and oxygen co-exposure in an ultrahigh vacuum (UHV) system. A dramatic enhanced degradation due to co-exposure of light and oxygen was observed. The chemical compositional changes of the sample were monitored with X-ray photoelectron spectroscopy (XPS). The exposure parameters such as pressure and time were carefully controlled and the exposure to oxygen was measured in Langmuir (L, 1 L = 10^{-6} Torr·s). Scanning electron microscopy (SEM) confirmed the high quality of the crystal and provided the change of morphological property. A focused ion beam (FIB) was also applied to perform depth profiling and gained insights into the bulk part of the crystal. A possible degradation path was proposed to explain the decomposition process. The DFT calculations were carried out to explain the experimental results and provide further insight. The photoluminescence (PL) indicates that oxygen could enhance the PL performance of $MAPbBr_3$ single crystal, while the combination of light and oxygen would deteriorate PL emission significantly.

Methods

The $MAPbBr_3$ single crystal was synthesized and provided by the collaborative group. The detailed fabrication method can be found in ref 13. The crystal has a translucent orange color and was cut into smaller ones with an average size of ~5 mm × 5 mm × 5 mm. The whole exposure process was conducted in a vacuum exposure chamber to rule out the effects from the ambient environment. The crystal was cleaved in-situ to obtain an uncontaminated pristine surface. (Fig. S1.) The sample was put into a vacuum desiccator to proceed to the PL measurement after the exposure. The PL measurements were performed ex-situ at room temperature under atmospheric pressure. For SEM and FIB measurement, the pristine sample was cleaved ex-situ right before putting into the instrument to have minimal exposure to the ambient environment on the crystal.

The configuration of our UHV system used for this study is shown in Fig. S2. It consists of two major chambers. One is the exposure chamber with a base pressure of 1 × 10^{-6} Torr used for cleaving and exposure. The other is the analysis chamber with a base pressure of 1 × 10^{-10} Torr used for XPS measurement. The light illumination was from a blue continuous wave (CW) laser which was attached to a viewport on the exposure chamber. It has a wavelength of 408 nm and the intensity was adjusted to equivalent to seven standard solar irradiances (1000 W·m^{-2} = 1.0 mW·mm^{-2}). Oxygen was fed in through a leak valve on the exposure chamber, which was connected to an ultrapure carrier-grade O_2 cylinder from Airgas Inc. The whole exposure process consisted of 13 steps. Details of exposure time and oxygen pressure of each step can be found in Table 1. The sample was immediately transferred to the analysis chamber for XPS measurement after each step. A microscope was mounted on the analysis chamber to monitor the XPS measuring spot, ensuring that each measurement was conducted on the same spot.

Table 1. Light and oxygen co-exposure detail

# of Exposure	Exposure (L)	Oxygen pressure (Torr)	Exposure Time (Second)
1	0	0	0
2	10^3	1×10^{-4}	10
3	10^4	2×10^{-3}	5
4	10^5	1×10^{-2}	9
5	10^6	0.1	9
6	10^7	1	9
7	10^8	10	9
8	10^9	100	9
9	10^{10}	760	12
10	10^{11}	760	118
11	10^{12}	760	1184
12	2×10^{12}	760	2368
13	4×10^{12}	760	4736

The XPS was equipped with a monochromatic Al Kα source (1486.6 eV) and was running at 10 kV and 20 mA. The spectra for each element were collected to estimate the elemental ratio of the sample surface by comparing the areas of the fitted curves divided by their atomic sensitivity factors. CasaXPS version 2.3 was used to fit the core level peak of each element and obtain their area of the fitted curve. Sample's morphology and depth profiling was investigated with a Zeiss Auriga FIB-SEM. Photoluminescence measurements were carried out on a Princeton Instruments

TriVista Triple Spectrometer system with a 355 nm ultraviolet laser as the excitation source.

All DFT calculations were performed with Quantum-ESPRESSO package, using the generalized gradient approximation (GGA) of Perdew–Burke–Ernzerhof exchange-correlation functional and the ultrasoft scalar relativistic pseudopotentials.[47, 48] A plane-wave kinetic energy cutoff of 50 and 200 Ry for the wave functions and the charge density, and a k-point mesh of 6 × 6 × 3 were used for these calculations. The MABr-terminated (110) perovskite slab model has a 2 × 2 × 2 structure containing 8 unit cells of $MAPbBr_3$ with a = b = 11.80 Å, and c = 26.80 Å, given $MAPbBr_3$ lattice constant of 5.90 Å and a vacuum region of 15 Å.[49]

Results and discussion

The $MAPbBr_3$ single crystals used in this study have been previously studied with X-ray diffraction (XRD), which confirm that the crystals had a highly crystalline cubic structure with a lattice constant of 5.90 Å.[13, 22, 32, 49] The XPS survey scan of the as-cleaved sample is shown in Fig. 1c and all core level peaks are marked. All detected elements were associated with the perovskite and no oxygen or silver from the residual silver paste. The results suggest that the as-cleaved sample was pure and not contaminated. The elemental ratio of C/N/Pb/Br is 1.30/1.06/1/2.67, where Pb was set as 1 to be compared with. This ratio is close to the ideal stoichiometric value. The little bromine deficiency could be due to Br vacancies on the crystal surface and the small amounts of excess carbon and nitrogen may be attributed to the residual reactants used in the sample growth process.

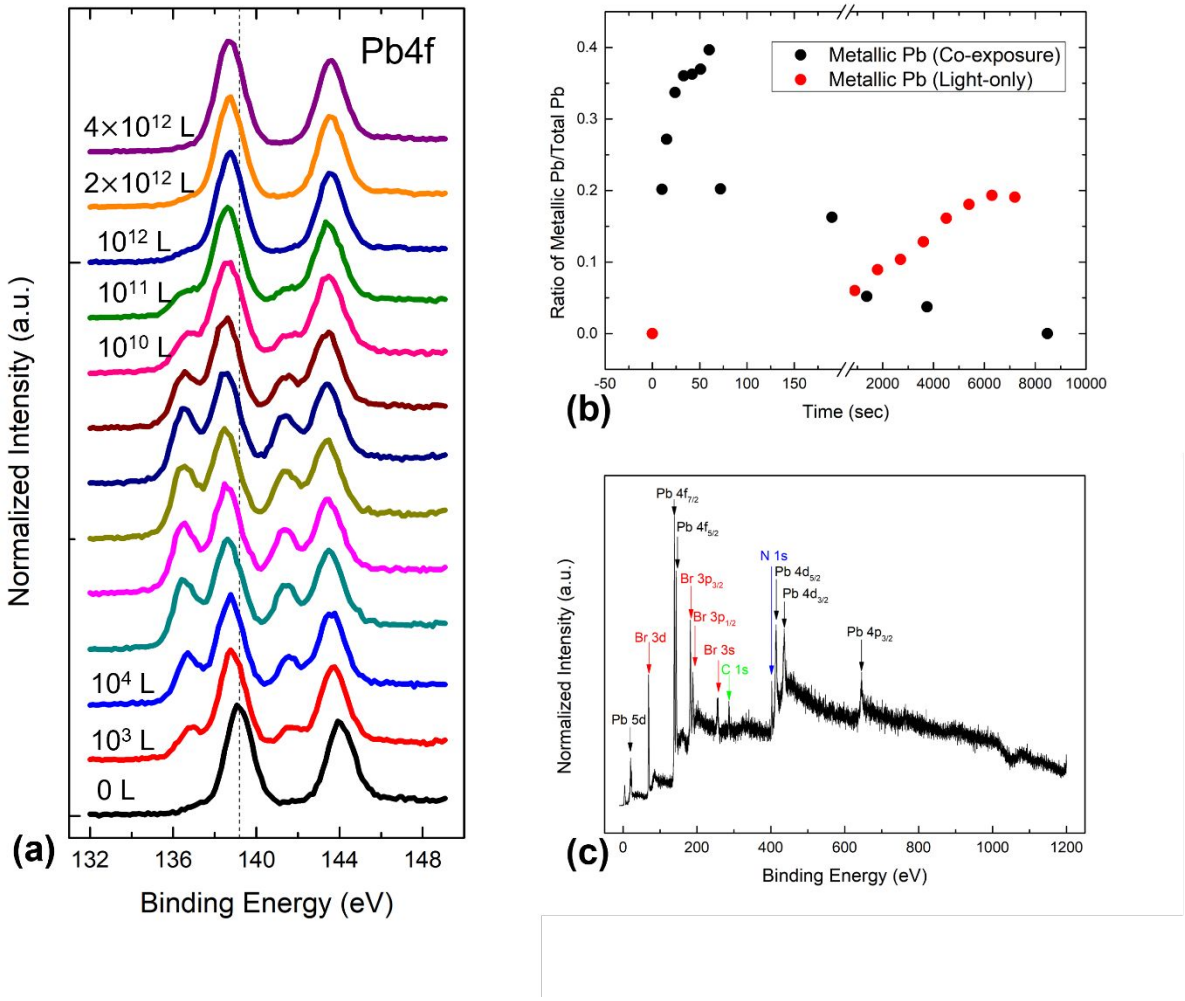

Fig. 1 (a) Evolutions of Pb 4f XPS spectra with increasing light and oxygen co-exposure. (b) Metallic Pb ratio trend comparison for co-exposure and light-only exposure. The metallic Pb ratio was obtained by using metallic Pb peak intensity divided by the total Pb intensity. (c) XPS survey spectrum of as-cleaved $MAPbBr_3$ single crystal.

ARTICLE

The spectra evolution of the Pb core level during the exposure is shown in Fig. 1a. The XPS spectra have been normalized to the same maximum height for visual clarity. To provide full information of the spectra, the normalization factors of each core levels are presented in Table S1. The initial perovskite Pb $4f_{7/2}$ and $4f_{5/2}$ core levels were located at 139.15 and 144.03 eV, respectively. After co-exposure starts, a new Pb feature quickly began to develop for both Pb core levels and continue to grow in intensity until 10^9 L. The new feature was about 2.0 eV lower in binding energy (BE) from the perovskite Pb. Both new and the original Pb components shifted to a lower BE during the co-exposure with a BE of ~0.46 eV. Similar to Pb, this downward-moving pattern was also seen in C, N, Br core levels and valence band maxima (VBM). (Fig. 2) Therefore, the BE shift indicates a p-doping of perovskite as the Fermi level moves closer to the valence band. This can be explained by the formation of reversible photoinduced p-type traps or the n-type trap reduction caused by photogenerated charge carriers on the sample surface.[50]

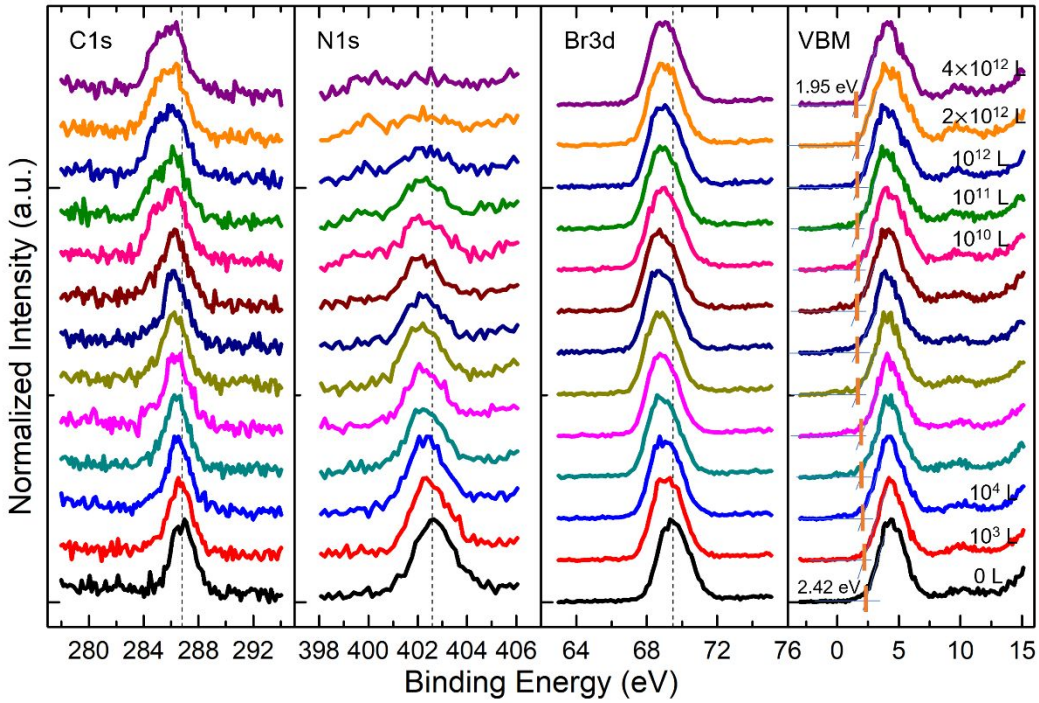

Fig. 2 A stack plot of the C 1s, N 1s, Br 3d core levels and VBM with increasing oxygen and light co-exposure. Each spectrum was normalized to one for perspective.

The original Pb $4f_{7/2}$ component continued to move downward in BE and reached the lowest position of 138.53 eV at 10^9 L and the new Pb component's ratio grew rapidly from 0 to 0.40 within first 72 seconds (10^9 L), representing a significant chemical change on the surface (Fig. 1b). This new Pb feature represents the formation of a new Pb species, which has previously been reported as metallic Pb.[30, 34, 51, 52] It also has been reported that the metallic Pb could deteriorate the performance of the device as an exciton quencher and enhance the nonradiative recombination.[51] In contrast, light-only sample shows a much slower degradation rate as its metallic Pb took ~8 hours to reach a 0.40 ratio (Fig. S3). After 10^9 L exposure, the ratio of metallic Pb began to decrease as shown in Fig. 1b. This observation is significantly different from our previous light-only exposure, where metallic Pb continued to develop and eventually became the dominant Pb feature, representing 70% of the overall Pb signal.[30] The

reduction of metallic Pb could be attributed to the formation of PbO as Anaya *et al.* observed the presence of PbO, after illumination of $MAPbBr_3$ in an oxygen environment.[53] There are also reports in the literature that studied the Pb oxidation process.[54-57] Oxygen could form superoxide species under illumination by grabbing electrons from perovskite, then hydrogen peroxide (H_2O_2) can be generated from the reactions of hydroperoxyl, water, and oxygen.[54] Peroxide anion, a strong oxidant could react with metallic Pb and form PbO on the perovskite surface.

In Fig. 2, the XPS spectra of the other perovskite elements, C, N, Br and VBM region are presented. The XPS spectra have been normalized to the same maximum height for visual clarity. Unlike Pb, there is no emerging component in Br 3d, which suggests no change in the chemical state of these elements. While C 1s developed a secondary peak at 284.7 eV after 10^{10} L, attributed to the formation of C-O bond as the oxygen pressure increases. A small secondary N 1s peak merged at 399 eV after 10^{10} L, indicating the reaction between perovskite and H_2O formed under light illumination. These changes are consistent with our previous observations.[32] They all showed a BE shift of ~0.46 eV toward lower BE region, confirming the p-doping of the surface. The detailed BE shift and peak fitting can be found in Fig. S4. However, the intensity of these elements experienced significant losses in the concentrations with increasing exposure. As shown in Fig. 2 and Fig. 3b, at 10^{12} L of exposure, C, N, and Br ratio dropped to 54%, 17% and 51% of their initial concentration. With two more steps of exposure, the C and Br ratio did not change much, while N further dropped to only 4% of its initial concentration, suggesting that the perovskite surface has fully decomposed. This degradation process was much faster than that in the light-only exposure. On the contrary, in Fig. 3a, there was no oxygen detected before 10^{10} L, then started to rapidly develop at 533.09, 529.26 and 531.20 eV, and the ratio was also increased to 0.08, 0.13 and 0.07 respectively. (Fig. 3c) This oxygen surge was caused by the increasing oxygen pressure to 760 Torr (1 atm), leading to the formation of PbO as previously discussed. The three oxygen peaks indicate that there were three different types of oxygen states, which are assigned to H_2O at 533 eV, superoxide PbO_2 at 530 eV, and oxide PbO at 529 eV..[58] (See Fig. S5 for detailed fitting) From the data presented in Fig. 3c, the amount of the oxide and superoxide is about 17 percent of the atomic ratio with respect to Pb, about half of that of metallic Pb. Although we observed a strong correlation between the decrease of metallic Pb and the increase of O, it appeared that not all the removal of the metallic Pb could be counted for by the oxide and peroxide formation. One of the possible explanations for this apparent quantitative discrepancy is that the metallic Pb and its oxidation occur at the very top of the surface, whereas the total Pb signal is from a semi-infinite slab of the sample from the surface science point of view. The photoelectron attenuation will therefore over-emphasize the signal from the top layer with respect to that of the bulk, leading to an apparently higher percentage of metallic Pb. Other possible contributing factors include that some of the metallic Pb may react with the remnant of the perovskite as the co-exposure has led to substantial change in the surface area of the sample as shown in Fig. 3b, or diffuse into the bulk of the sample during the long experiment. Fig. 3c shows that superoxides and oxides exhibit a faster rate of increase, whereas the water content gradually increases. It agrees well with the conclusion that water is the product of the peroxide and methylammonium.[53] The lost substance of C, N, and Br could leave the sample surface in a form of volatile species.[30] Based on the discussion above, the degradation process of $MAPbBr_3$ can be expressed as the following equations:

$$CH_3NH_3PbBr_3 \xrightarrow{Light} Pb + CH_3NH_3Br\uparrow + Br_2\uparrow$$

$$Pb + H_2O_2 \rightarrow PbO + H_2O$$

Where the formation of hydrogen peroxide can be attributed to either the reaction of superoxide with water or hydroperoxyl radical electron abstraction.[54] In our previous oxygen-only exposure, the perovskite surface only saw about 10% of perovskite Pb converted to metallic Pb at 10^{10} L which suggests that 10% of perovskite on the surface was degraded and oxygen doesn't react with $MAPbBr_3$ as it only acts as p-dopant.[32] (Fig. S6) In order to determine oxygen's role in oxygen and light co-exposure, we compared the co-exposure with the similar amount of exposure time as the previous light-only exposure. The ratio comparison of light-only exposure with co-exposure is shown in Table 2. Both exposures started with very close ratios from two different samples, which again confirmed the high quality of the crystal. After 30 minutes of light-only exposure, C, N, and Br ratio dropped to 1.18/0.92/2.41, which represents 23.3%, 14.0%, and 6.6% losses of their initial concentration respectively. It further dropped to 1.16/0.81/2.07 and the concentration losses were increased to 24.7%, 24.3%, and 19.8% respectively. Compared to the co-exposure, it's obvious that the degradation process with light-only was much slower. In other words, the presence of oxygen had accelerated the degradation. As for metallic Pb, it kept growing with the light-only-exposure, became the dominant Pb component after 10 hours and eventually saturated with a composition of 64% of total Pb ratio. (Fig. S3) In comparison, metallic Pb peaked at 60 seconds (10^8 L) with a ratio of 0.37, then quickly re-oxidized with increasing oxygen pressure. At 10^{10} L, the co-exposed sample lost 69% of its initial nitrogen, while the oxygen-only exposed one only saw a 3% drop. The light exposure was 72 seconds (see Table 1). From the light-only exposure data presented in Fig. 3b, we extrapolated the nitrogen loss after 72 seconds of light exposure to be approximately 1% of the initial concentration, and the additive effect of light-only and oxygen-only exposures on nitrogen should be 4%. The

nitrogen loss due to co-exposure is therefore 17.25 times that of the additive effect, demonstrating significantly higher enhancement of degradation by co-exposure.

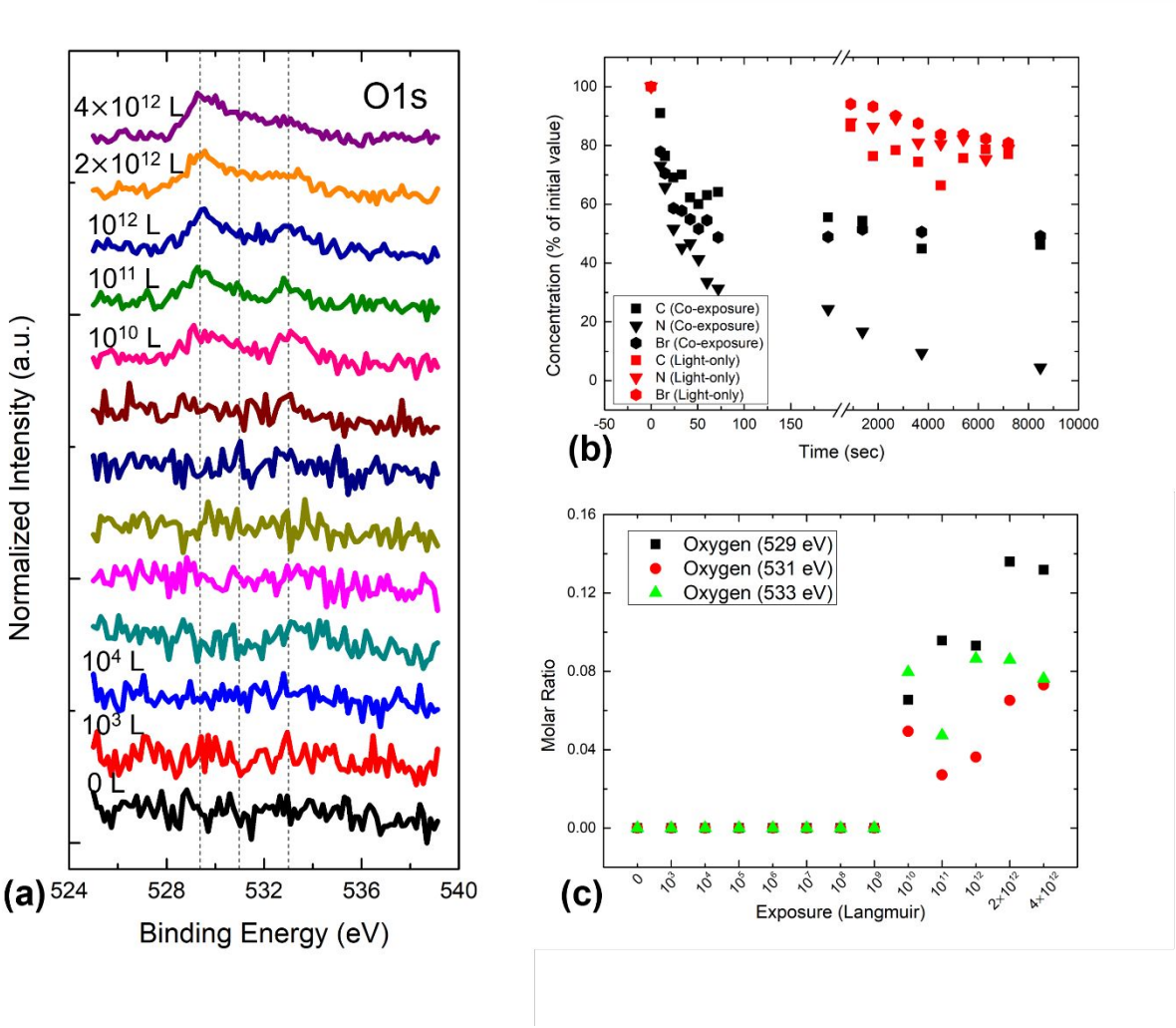

Fig. 3. (a) A stack plot of the O 1s core levels with increasing oxygen and light exposure. The three oxygen peaks formed after 10^{10} L are assigned to H_2O at 533 eV, O_2^- / O_2^- /OH^- at 530 eV ,and physical absorbed oxygen (O_2) at 529 eV Each spectrum was normalized to one for perspective. (b) Ratio trend comparison of C, N and Br for co-exposure and light-only exposure. It shows a much faster concentration loss in the co-exposure. (c) O ratio trend for three peak components oxide O^{2-} (529 eV), superoxide O_2^- (530 eV) and H_2O (533 eV). The oxygen ratios show a significant increase as co-exposure evolves.

Table 2. Ratio comparison of light-only exposure with light and oxygen co-exposure.

Ratio	Br	Pb/Metallic Pb	C	N
As-cleaved (Light-only)	2.58	1/0	1.54	1.07
As-cleaved (Co-exposure)	2.67	1/0	1.30	1.06
30 min (Light-only)	2.41	0.91/0.09	1.18	0.92
24 min (10^{12} L of co-exposure)	1.37	0.95/0.05	0.71	0.18
150 min (Light-only)	2.07	0.79/0.21	1.16	0.81
141min (4×10^{12} L of co-exposure)	1.31	1/0	0.60	0.05

Formation of superoxide plays a critical role in the degradation process. We conducted the DFT calculation to have a better understanding of the charge redistribution between $MAPbBr_3$ and oxygen. We examined three oxygen absorption sites on MABr terminated surface: hollow-site, MA-site (close to MA cation) and Br-site (close to Br cation). After structural optimization of the pristine model, the oxygen molecule was manually added to each absorption site. The charge density difference was obtained via following formula:

$$\Delta\rho = \rho_{MAPbBr+O_2} - \rho_{O_2} - \rho_{MAPbBr}$$

Where $\rho_{MAPbBr+O_2}$is the charge density of oxygen-absorbed model, and ρ_{O_2}, ρ_{MAPbBr} are the charge density of individual oxygen molecule and $MAPbBr_3$, respectively. The calculated charge density difference is shown in Fig. 4a. The yellow contour surface shows the gaining of electrons while the cyan ones indicate electron loss. Apparently, hollow-site gains more electrons than other two absorption sites in the occupied orbital, which suggesting that hollow site is the optimized position for the oxygen interaction and it's in line with existing $MAPbI_3$ work.[44] We propose that the significant spatial overlap observed between the occupied and unoccupied orbitals near O_2 indicates the potential for high transition rates during optical excitation. This phenomenon is likely to lead to the formation of O radicals as a consequence. This may lead to a higher probability for an electron to transfer from an occupied to an unoccupied orbital when the model is exposed to light. Thus, charge transfer between perovskite and O_2 will be promoted with light illumination, then favors the formation of superoxide species and eventually enhance the breakdown of perovskite. The photolytic generation of oxygen radials in perovskites with the light absorption has been reported in many existing literatures.[53, 57, 59] Our DFT calculations and XPS measurements only provide the ground state information, and further investigations sensitive to the exited states may also be needed. In addition, we also calculated density of states (DOS) of the pristine model and three oxygen absorbed models (Fig. 4b), the pristine $MAPbBr_3$ model shows a bandgap of 2.26 eV, which is very close to the experimental 2.30 eV bandgap. The calculated Fermi level was set to be 0 eV for the pristine model, so the VBM with respect to Fermi level are -1.01, -1.09 and -0.73 eV for the hollow-site, MA-site and Br-site models, respectively. It suggests that the oxygen moved the Fermi level lower in the bandgap which p-doped the sample. This result qualitatively agrees with our experimental observation as the XPS core level peaks shifted ~0.46 eV lower after the exposure. The BE movement at Br-site is 0.40 eV, given the calculated bandgap of 2.26 eV. The smaller simulated BE movement can be explained that our experimental sample has an initial Pb-rich surface due to the Br vacancies, leading to the self p-doping.[60] Thus, the initial p-doping could contribute to the overall larger BE movement of the experimental sample. The similar bandgap of the four models shows the introduction of an oxygen molecule to the system has little effect on the bandgap. Our excitation source is a blue continuous wave laser with a wavelength of 408 nm, which is equivalent to a photon energy of 3.04 eV. The mid-gap states introduced by oxygen were localized at -0.96, -1.10 and -0.74 eV below the Fermi level for hollow, MA and Br sites, and can be easily photoexcited to the unoccupied states by the light illumination As a result of O^{2-} photo ionization, a radical species $O_2^- \cdot$ is generated that is highly reactive, leading to the formation of various defect states and enhancing the degradation of the perovskite. Considering the energy of oxygen mid-gap states in the bandgap, this degradation enhancement should also happen for photon energies greater than 1.77 eV. In the actual experimental conditions, the oxygen-induced gap states should appear as a broader feature since the absorptions occur more randomly than in our four configured sites. The experimental VBM spectra shown in Fig. S7 reveals that the intensity was elevated between Fermi level and the VBM, resulting from the oxygen adsorption on the surface. Furthermore, the shift of the VBM towards a lower binding energy region is consistent with our earlier discussion. Fig. S8 shows the projected density of states (PDOS) of four oxygen adsorption sites. It clearly shows that the mid-gap states are introduced by oxygen. The unoccupied region is primarily formed by Pb orbitals in all four sites without oxygen contributions, while occupied region was mostly from Br orbitals.

ARTICLE

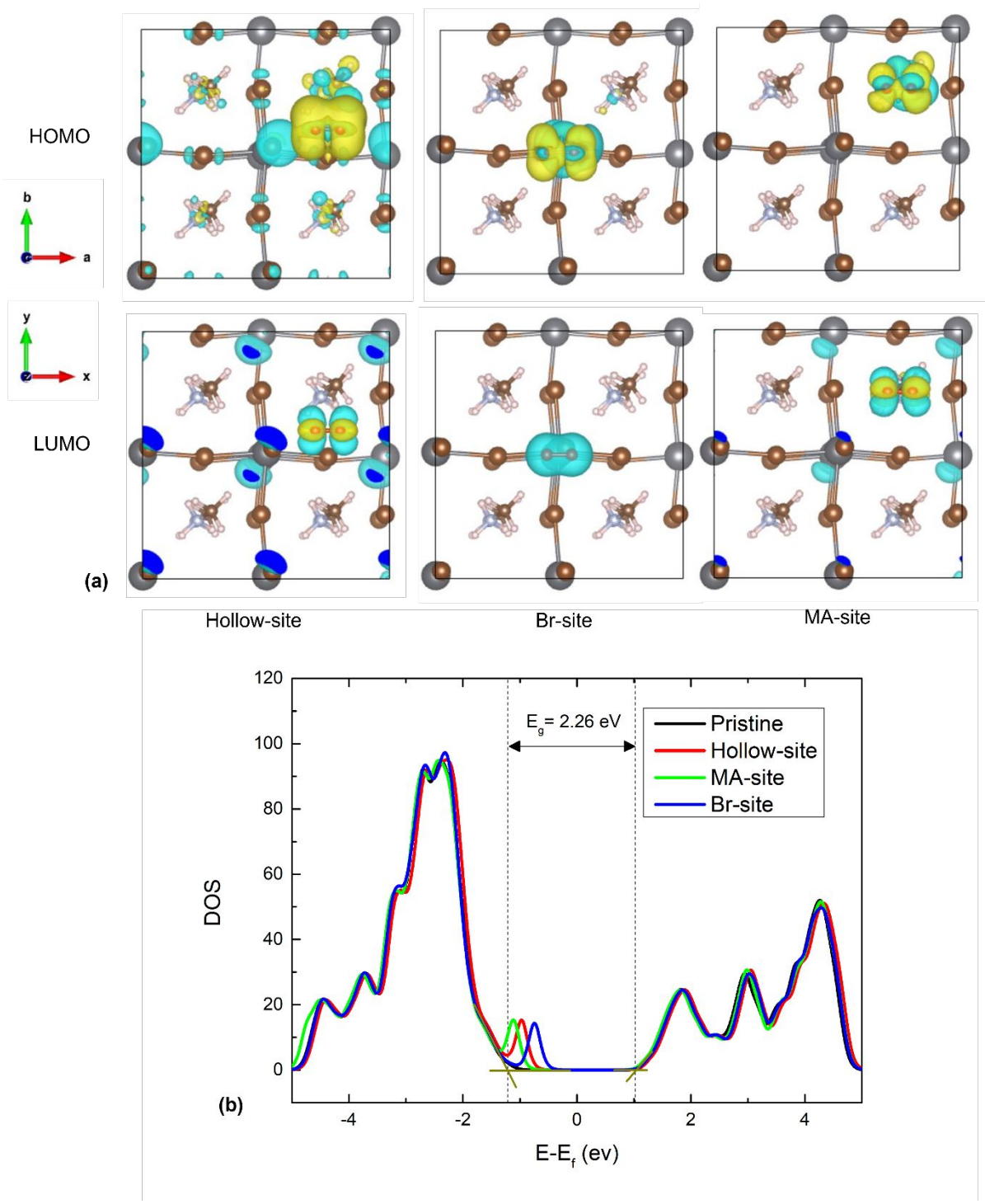

Fig. 4. (a) Top views of charge density difference of three oxygen-absorption sites. (b) Density of states comparisons of pristine model and three oxygen absorbed models.

ARTICLE

During the co-exposure, we observed a green emission of the sample. (See Fig. S9) To investigate this photoemission, the sample was characterized by PL. The PL spectra of the pristine sample and the two exposed ones are presented in Fig. 5. All of the three spectra have a similar emission peak at ~ 540 nm with full width at half-maximum (FWHM) of ~23 nm. The emission peak at 540 nm confirms the green emission from the previous observation. It is also comparable to the emission peak measured on $MAPbBr_3$ thin films and quantum dots.[61, 62] However, the PL intensities of these three conditions are quite different. For oxygen-only exposure, the PL intensity increased 78.7% compared to that of the pristine one, whereas it decreased 83.5% for the light and oxygen co-exposure sample. Clearly, the poor performance of the co-exposed sample was due to the accelerated degradation, which severely damaged the perovskite structure as most carbon, nitrogen, and the majority of bromine escaped the sample surface. Also, metallic Pb serves as quenching centers of excitons and have detrimental effect on the PL quantum efficiency.[51] The PL enhancement by oxygen exposure agrees with many existing studies. [14, 53, 63, 64] This can be explained that O_2^- formed by absorption of oxygen on the perovskite surface drives halide anions migrate toward bulk part, which reduces bulk halide vacancies. Therefore, the reduction of trap states in the bulk of the perovskite could be the main reason of the PL enhancement.

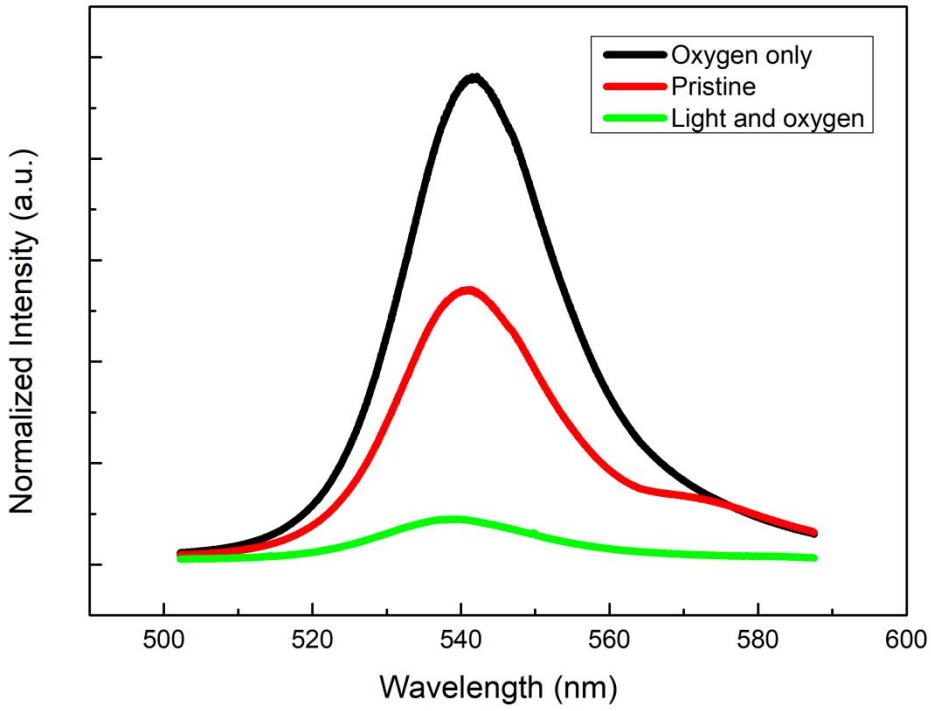

Fig. 5. PL spectra of oxygen-only exposed, light and oxygen co-exposed, and pristine samples.

Morphological properties and depth profiling of the crystal were investigated with SEM and FIB and the results are shown in Fig. 6. The freshly cleaved sample has a smooth and featureless surface shown in Fig. 6a, while the co-exposed surface in Fig. 6b was significantly roughened and transformed. White dots on the surface could be the generated PbO during the degradation, as the nanoparticles are visually similar to the observation by Minigalieva *et al.*[65] However, the co-exposed surface still looks more uniform than the light-only exposed surface from the previous work, which was covered with large spherical clusters that were the metallic Pb caused by the

degradation.[30] FIB was used to create microscopic trenches with a depth of 2-3 µm. As shown in Fig. 6c and d, both samples have no voids or any other features below the surface, indicating that the bulk part of the crystals remained unaltered. This result is quite different from our previous 44-hour light-only work observed that large voids were seen 1–3 µm down into the material in the light-exposed region, which were caused by the light exposure. The formation of these voids was previously reported as the result of the Kirkendall effect, suggesting that the voids were created by the irreversible chemical reactions from undesired diffusion under light illumination.[30] The missing of the voids in the co-exposure could be explained by the limitation of exposure time, as the total exposure time for the co-exposure was only 141 minutes compared with 44-hour light-only exposure. Given the limited exposure time, we expect that the metallic Pb and its oxidation to occur primarily at the top few atomic layers of the surface. Another possibility is that the co-exposure induced surface degradation hindered the diffusion under light illumination. In either case, the diffusion process in the bulk part of the crystal may not be enough to form the voids.

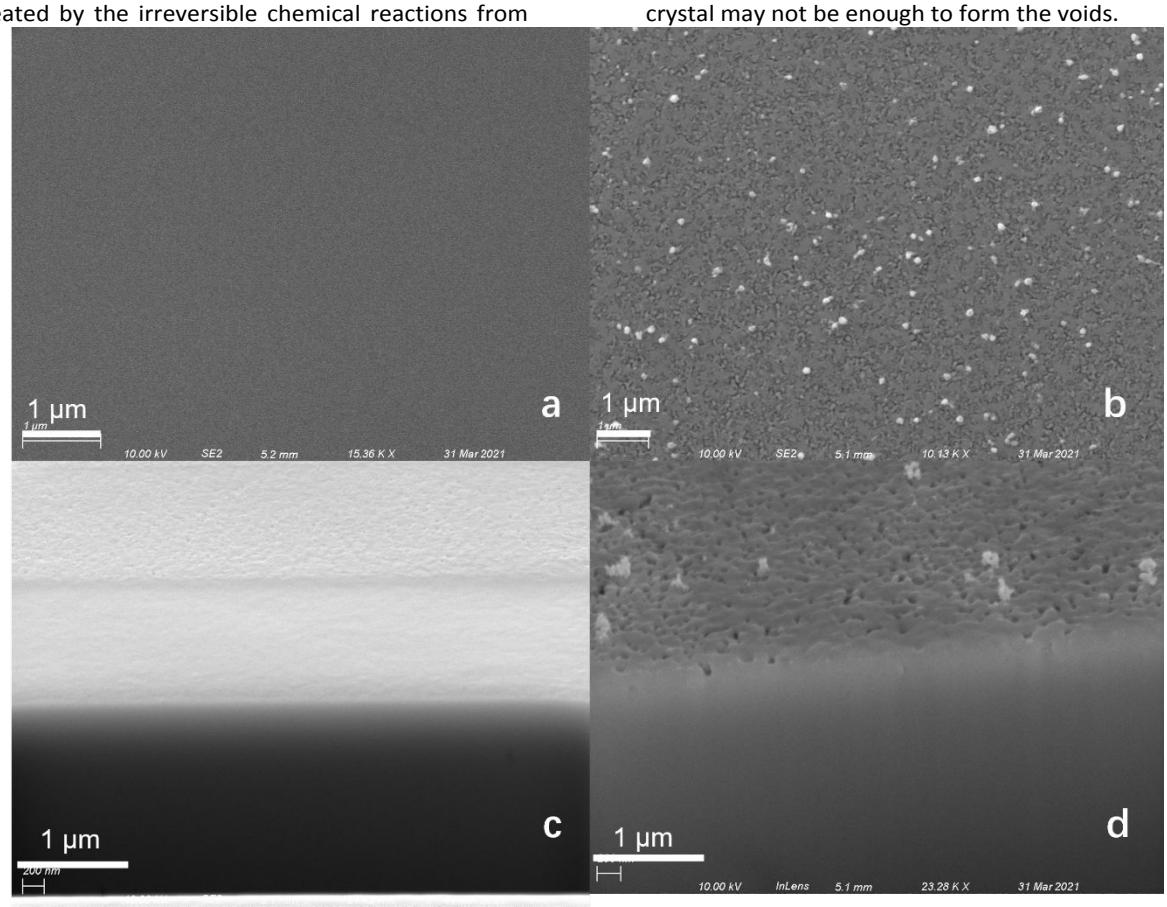

Fig. 6. (a)(b) The SEM image of the surface of the freshly cleaved and the exposed samples respectively. (c)(d) The FIB milled trenches for the freshly cleaved and the exposed samples respectively. The FIB milled trench of the exposed region revealed about 2 µm deep into the material.

Conclusions

In summary, we have studied light-enhanced oxygen degradation of $MAPbBr_3$ single crystal. This quantitative and systematic investigation was carried out at the surface level in UHV condition. Compared to exposure to oxygen-only or light-only exposures, the light and oxygen co-exposure substantially accelerated the degradation process of $MAPbBr_3$ as evidenced by the more rapid decrease in the ratios of C, N, and Br, which is attributed to the presence of the superoxides. It suggests that C, N, and Br were formed into volatile species then leave the surface. We observed that a small portion of Pb was initially converted into metallic Pb, then oxidated with increasing oxygen pressure. At 10^{10} L, the enhanced degradation is 17.25 times the simple additive effect of light-only and oxygen-only exposure, in terms of nitrogen loss. DFT calculations further confirms that the formation of superoxide, which leads to the photoexcitation to oxygen radicals and enhancement of the degradation by the co-exposure. SEM and FIB results showed that the exposed area of the surface was roughened but the bulk part remained intact, which may also explain a significantly decreased PL performance. We believe this work has revealed the chemical and morphological effects resulting from the co-exposure of light and oxygen. These findings can help to build a better understanding of the degradation process of perovskite in real environments, thus taking a step forward towards finding a solution for perovskite stability issues.

Author Contributions

Ke Wang: conceptualization, investigation, data curation, methodology, formal analysis, writing – original draft. Benjamin Ecker: conceptualization. Maitrayee Ghosh: data curation, software, writing – review & editing. Mingze Li: writing – review & editing. Valentin V. Karasiev: software, writing – review & editing. S. X. Hu: resources, writing – review & editing. Jinsong Huang: resources, writing – review & editing. Yongli Gao: conceptualization, supervision, resources, writing – review & editing.

Conflicts of interest

The authors declare no conflict of interest.

Acknowledgements

The work receives financial support from National Science Foundation (Grant # DMR-1903962). B.E. acknowledges Hooker Dissertation Fellowship from the University of Rochester. M.G., V.V.K., and S.X.H. acknowledge the support by the Department of Energy National Nuclear Security Administration under Award No. DE-NA0003856. The authors would like to thank URnano center and Multiwavelength Raman Spectroscopy Facility at University of Rochester for technical support with SEM, FIB and PL measurements.

References

1. H. J. Snaith, *The Journal of Physical Chemistry Letters*, 2013, **4**, 3623-3630.
2. D. Liu and T. L. Kelly, *Nature Photonics*, 2013, **8**, 133-138.
3. Y. K. Wang, Z. C. Yuan, G. Z. Shi, Y. X. Li, Q. Li, F. Hui, B. Q. Sun, Z. Q. Jiang and L. S. Liao, *Advanced Functional Materials*, 2016, **26**, 1375-1381.
4. H. Xie, X. Liu, L. Lyu, D. Niu, Q. Wang, J. Huang and Y. Gao, *The Journal of Physical Chemistry C*, 2015, **120**, 215-220.
5. H. S. Kim, C. R. Lee, J. H. Im, K. B. Lee, T. Moehl, A. Marchioro, S. J. Moon, R. Humphry-Baker, J. H. Yum, J. E. Moser, M. Gratzel and N. G. Park, *Sci Rep*, 2012, **2**, 591.
6. W. A. Dunlap-Shohl, R. Younts, B. Gautam, K. Gundogdu and D. B. Mitzi, *The Journal of Physical Chemistry C*, 2016, **120**, 16437-16445.
7. A. Abrusci, S. D. Stranks, P. Docampo, H. L. Yip, A. K. Jen and H. J. Snaith, *Nano Lett*, 2013, **13**, 3124-3128.
8. S. D. Stranks, G. E. Eperon, G. Grancini, C. Menelaou, M. J. P. Alcocer, T. Leijtens, L. M. Herz, A. Petrozza and H. J. Snaith, *Science*, 2013, **342**, 341-344.
9. K. Wang, B. Ecker, J. Huang and Y. Gao, *Nanomaterials*, 2021, **11**, 2532.
10. K. Wang, B. Ecker and Y. Gao, *Crystals*, 2020, **10**, 773.
11. Z.-K. Tan, R. S. Moghaddam, M. L. Lai, P. Docampo, R. Higler, F. Deschler, M. Price, A. Sadhanala, L. M. Pazos and D. Credgington, *Nature nanotechnology*, 2014, **9**, 687-692.
12. X. Li, D. Bi, C. Yi, J.-D. Décoppet, J. Luo, S. M. Zakeeruddin, A. Hagfeldt and M. Grätzel, *Science*, 2016, **353**, 58-62.
13. H. Wei, Y. Fang, P. Mulligan, W. Chuirazzi, H.-H. Fang, C. Wang, B. R. Ecker, Y. Gao, M. A. Loi and L. Cao, *Nature Photonics*, 2016, **10**, 333-339.
14. H.-H. Fang, S. Adjokatse, H. Wei, J. Yang, G. R. Blake, J. Huang, J. Even and M. A. Loi, *Science Advances*, 2016, **2**, e1600534.
15. Y. Fang, Q. Dong, Y. Shao, Y. Yuan and J. Huang, *Nature Photonics*, 2015, **9**, 679-686.
16. W. Chen, Z. Huang, H. Yao, Y. Liu, Y. Zhang, Z. Li, H. Zhou, P. Xiao, T. Chen and H. Sun, *Nature Photonics*, 2023, 1-7.
17. Q. Xu, H. Wei, W. Wei, W. Chuirazzi, D. DeSantis, J. Huang and L. Cao, *Nuclear Instruments and Methods in Physics Research Section A: Accelerators, Spectrometers, Detectors and Associated Equipment*, 2017, **848**, 106-108.
18. L. C. Schmidt, A. Pertegas, S. Gonzalez-Carrero, O. Malinkiewicz, S. Agouram, G. Minguez Espallargas, H. J. Bolink, R. E. Galian and J. Perez-Prieto, *J Am Chem Soc*, 2014, **136**, 850-853.
19. T. Baikie, Y. Fang, J. M. Kadro, M. Schreyer, F. Wei, S. G. Mhaisalkar, M. Graetzel and T. J. White, *Journal of Materials Chemistry A*, 2013, **1**, 5628-5641.
20. R. Ohmann, L. K. Ono, H.-S. Kim, H. Lin, M. V. Lee, Y. Li, N.-G. Park and Y. Qi, *Journal of the American Chemical Society*, 2015, **137**, 16049-16054.
21. Y. Liu, Y. Zhang, K. Zhao, Z. Yang, J. Feng, X. Zhang, K. Wang, L. Meng, H. Ye and M. Liu, *Advanced Materials*, 2018, **30**, 1707314.
22. C. Wang, B. R. Ecker, H. Wei, J. Huang, J.-Q. Meng and Y. Gao, *Physical Chemistry Chemical Physics*, 2017, **19**, 5361-5365.
23. Y. Yang, Y. Yan, M. Yang, S. Choi, K. Zhu, J. M. Luther and M. C. Beard, *Nature communications*, 2015, **6**, 1-6.
24. J. H. Heo, D. H. Song and S. H. Im, *Advanced Materials*, 2014, **26**, 8179-8183.
25. X. Dai, S. Chen, H. Jiao, L. Zhao, K. Wang, Z. Ni, Z. Yu, B. Chen, Y. Gao and J. J. N. E. Huang, 2022, **7**, 923-931.
26. B. Brunetti, C. Cavallo, A. Ciccioli, G. Gigli and A. Latini, *Scientific reports*, 2016, **6**, 1-10.
27. A. Alberti, I. Deretzis, G. Mannino, E. Smecca, S. Sanzaro, Y. Numata, T. Miyasaka and A. La Magna, *The Journal of Physical Chemistry C*, 2017, **121**, 13577-13585.
28. J. A. Christians, P. A. Miranda Herrera and P. V. Kamat, *Journal of the American Chemical Society*, 2015, **137**, 1530-1538.
29. Y.-H. Kye, C.-J. Yu, U.-G. Jong, Y. Chen and A. Walsh, *The journal of physical chemistry letters*, 2018, **9**, 2196-2201.
30. B. R. Ecker, C. Wang, H. Wei, Y. Yuan, J. Huang and Y. Gao, *Advanced Materials Interfaces*, 2018, **5**.
31. C. Wang, Y. Li, X. Xu, C. Wang, F. Xie and Y. Gao, *Chemical Physics Letters*, 2016, **649**, 151-155.

32. C. Wang, B. R. Ecker, H. Wei, J. Huang and Y. Gao, *The Journal of Physical Chemistry C*, 2018, **122**, 3513-3522.
33. Y. Li, X. Xu, C. Wang, C. Wang, F. Xie, J. Yang and Y. Gao, *The Journal of Physical Chemistry C*, 2015, **119**, 23996-24002.
34. Q. Jiang, Z. Chu, P. Wang, X. Yang, H. Liu, Y. Wang, Z. Yin, J. Wu, X. Zhang and J. You, *Advanced materials*, 2017, **29**, 1703852.
35. K. Wang, B. Ecker and Y. Gao, *Energies*, 2021, **14**, 2005.
36. K. Wang, B. Ecker, M. Li, J. Huang and Y. J. T. J. o. P. C. C. Gao, 2023, **127**, 19599-19606.
37. G. E. Eperon, S. D. Stranks, C. Menelaou, M. B. Johnston, L. M. Herz, H. J. J. E. Snaith and E. Science, 2014, **7**, 982-988.
38. M. M. Lee, J. Teuscher, T. Miyasaka, T. N. Murakami and H. J. J. S. Snaith, 2012, **338**, 643-647.
39. B. Suarez, V. Gonzalez-Pedro, T. S. Ripolles, R. S. Sanchez, L. Otero and I. J. T. j. o. p. c. l. Mora-Sero, 2014, **5**, 1628-1635.
40. T. Leijtens, G. E. Eperon, S. Pathak, A. Abate, M. M. Lee and H. J. J. N. c. Snaith, 2013, **4**, 1-8.
41. D.-Y. Son, J.-W. Lee, Y. J. Choi, I.-H. Jang, S. Lee, P. J. Yoo, H. Shin, N. Ahn, M. Choi and D. J. N. E. Kim, 2016, **1**, 1-8.
42. B. Murali, S. Dey, A. L. Abdelhady, W. Peng, E. Alarousu, A. R. Kirmani, N. Cho, S. P. Sarmah, M. R. Parida and M. I. Saidaminov, *ACS Energy Letters*, 2016, **1**, 1119-1126.
43. J. F. Galisteo-López, M. E. Calvo and H. Míguez, *ACS Applied Energy Materials*, 2019, **2**, 6967-6972.
44. Y. Ouyang, Y. Li, P. Zhu, Q. Li, Y. Gao, J. Tong, L. Shi, Q. Zhou, C. Ling and Q. Chen, *Journal of Materials Chemistry A*, 2019, **7**, 2275-2282.
45. Q. Sun, P. Fassl, D. Becker‐Koch, A. Bausch, B. Rivkin, S. Bai, P. E. Hopkinson, H. J. Snaith and Y. Vaynzof, *Advanced Energy Materials*, 2017, **7**, 1700977.
46. G. Abdelmageed, L. Jewell, K. Hellier, L. Seymour, B. Luo, F. Bridges, J. Z. Zhang and S. Carter, *Applied Physics Letters*, 2016, **109**, 233905.
47. P. Giannozzi, S. Baroni, N. Bonini, M. Calandra, R. Car, C. Cavazzoni, D. Ceresoli, G. L. Chiarotti, M. Cococcioni and I. Dabo, *Journal of physics: Condensed matter*, 2009, **21**, 395502.
48. J. P. Perdew, K. Burke and M. Ernzerhof, *Physical review letters*, 1996, **77**, 3865.
49. A. Poglitsch and D. Weber, *The Journal of chemical physics*, 1987, **87**, 6373-6378.
50. E. T. Hoke, D. J. Slotcavage, E. R. Dohner, A. R. Bowring, H. I. Karunadasa and M. D. McGehee, *Chemical Science*, 2015, **6**, 613-617.
51. G. Sadoughi, D. E. Starr, E. Handick, S. D. Stranks, M. Gorgoi, R. G. Wilks, M. Bär and H. J. Snaith, *ACS applied materials & interfaces*, 2015, **7**, 13440-13444.
52. L. Liu, J. A. McLeod, R. Wang, P. Shen and S. Duhm, *Applied physics letters*, 2015, **107**, 061904.
53. M. Anaya, J. F. Galisteo-Lopez, M. E. Calvo, J. P. Espinos and H. Miguez, *J Phys Chem Lett*, 2018, **9**, 3891-3896.
54. J. S. Godding, A. J. Ramadan, Y.-H. Lin, K. Schutt, H. J. Snaith and B. Wenger, *Joule*, 2019, **3**, 2716-2731.
55. L. Zhang and P. H.-L. Sit, *Journal of Materials Chemistry A*, 2017, **5**, 9042-9049.
56. X. Wang and L. Andrews, *The Journal of Physical Chemistry A*, 2005, **109**, 9013-9020.
57. N. Aristidou, I. Sanchez‐Molina, T. Chotchuangchutchaval, M. Brown, L. Martinez, T. Rath and S. A. Haque, *Angewandte Chemie International Edition*, 2015, **54**, 8208-8212.
58. N. X.-r. P. S. Database, *National Institute of Standards and Technology*, DOI: https://dx.doi.org/10.18434/T4T88K,.
59. N. H. Nickel, F. Lang, V. V. Brus, O. Shargaieva and J. J. A. E. M. Rappich, 2017, **3**, 1700158.
60. Q. Wang, Y. Shao, H. Xie, L. Lyu, X. Liu, Y. Gao and J. J. A. P. L. Huang, 2014, **105**.
61. S. Gonzalez-Carrero, L. C. Schmidt, I. Rosa-Pardo, L. Martínez-Sarti, M. Sessolo, R. E. Galian and J. Pérez-Prieto, *ACS omega*, 2018, **3**, 1298-1303.
62. Z.-Y. Zhang, H.-Y. Wang, Y.-X. Zhang, Y.-W. Hao, C. Sun, Y. Zhang, B.-R. Gao, Q.-D. Chen and H.-B. Sun, *Scientific reports*, 2016, **6**, 1-7.
63. K. Mantulnikovs, A. Glushkova, M. r. Kollár, L. s. Forró, E. Horváth and A. Sienkiewicz, *ACS Applied Electronic Materials*, 2019, **1**, 2007-2017.
64. H. Zhang, Y. Liu, H. Lu, W. Deng, K. Yang, Z. Deng, X. Zhang, S. Yuan, J. Wang and J. Niu, *Applied Physics Letters*, 2017, **111**, 103904.
65. I. A. Minigalieva, B. A. Katsnelson, V. G. Panov, L. I. Privalova, A. N. Varaksin, V. B. Gurvich, M. P. Sutunkova, V. Y. Shur, E. V. Shishkina and I. E. Valamina, *Toxicology*, 2017, **380**, 72-93.